OPEN ACCESS Freely available online

PLOS ONE

The Dynamics of Stress p53-Mdm2 Network Regulated by p300 and HDAC1

Akshit Arora[1☯], Saurav Gera[1☯], Tanuj Maheshwari[1☯], Dhwani Raghav[1], Md. Jahoor Alam[2], R. K. Brojen Singh[2]*, Subhash M. Agarwal[1]*

1 Bioinformatics Division, Institute of Cytology and Preventive Oncology, Noida, India, **2** Centre for Interdisciplinary Research in Basic Sciences, Jamia Millia Islamia, New Delhi, India

Abstract

We construct a stress p53-Mdm2-p300-HDAC1 regulatory network that is activated and stabilised by two regulatory proteins, p300 and HDAC1. Different activation levels of $p53$ observed due to these regulators during stress condition have been investigated using a deterministic as well as a stochastic approach to understand how the cell responds during stress conditions. We found that these regulators help in adjusting p53 to different conditions as identified by various oscillatory states, namely fixed point oscillations, damped oscillations and sustain oscillations. On assessing the impact of p300 on p53-Mdm2 network we identified three states: first stabilised or normal condition where the impact of p300 is negligible, second an interim region where p53 is activated due to interaction between p53 and p300, and finally the third regime where excess of p300 leads to cell stress condition. Similarly evaluation of HDAC1 on our model led to identification of the above three distinct states. Also we observe that noise in stochastic cellular system helps to reach each oscillatory state quicker than those in deterministic case. The constructed model validated different experimental findings qualitatively.

Citation: Arora A, Gera S, Maheshwari T, Raghav D, Alam MJ, et al. (2013) The Dynamics of Stress p53-Mdm2 Network Regulated by p300 and HDAC1. PLoS ONE 8(2): e52736. doi:10.1371/journal.pone.0052736

Editor: Masaru Katoh, National Cancer Center, Japan

Received February 23, 2012; **Accepted** November 21, 2012; **Published** February 20, 2013

Funding: Dr. Brojen Singh has received partial financial support for this work from University Grants Commission. However Dr. Subhash Agarwal has worked without any financial support from any funding agency. The funders had no role in study design, data collection and analysis, decision to publish, or preparation of the manuscript.

Competing Interests: The authors have declared that no competing interests exist.

* E-mail: brojen2k@yahoo.com (RKBS); smagarwal@yahoo.com (SMA)

☯ These authors contributed equally to this work.

Introduction

The p53 is a 20-Kb tumor suppressor gene located on the small arm of human chromosome 17 that acts as a hub for a network of signalling pathways essential for cell growth regulation and apoptosis. It comprises of 393 amino acids and is divided into several structural and functional domains: the transactivation domain (TAD; residues 1–40), the proline-rich domain (PRD; residues 61–94), the DNA-binding domain (DBD; residues 100–300), the tetramerization domain (4D; residues 324–355) and the C-terminal regulatory domain (CTD; residues 360–393) [1]. Over the recent years many names have been accredited to p53 viz. Guardian of the Genome [2]; Death Star [3] and Cellular Gatekeper [4] and is regulated by a number of cellular proteins [5]. It is well established that p53 is accountable for preventing improper cell proliferation and maintaining genome integration following genotoxic stress. In normal proliferating cells, p53 is kept in low concentrations and exists mainly in an inactive latent form with a short half-life of 15–30 minutes [6]. This is due to interaction between p53 and Mdm2 the predominant negative regulator of p53. However, cellular insults activates p53 and its level increases rapidly. The activation of p53 is a result of several posttranslational modifications including phosphorylation, acetylation, sumoylation and neddylation [7]. Phosphorylation of Ser-15 and 37 at the amino terminus of p53 prevents Mdm2 binding, thus stabilizing p53. Also phosphorylation at Ser-15 increases p53 affinity for p300, thus promoting acetylation of p53 carboxy terminal by p300 [8]. Further the p53 in-turn activates the p53-targeted genes including those involved in cell cycle arrest and DNA repair, as well as apoptosis and senescence related genes. The activation of the p53-targeted genes leads to cell cycle arrest that forces cell to choose either to repair the DNA damage to restore its normal function or cell death (apoptosis). Further, it has been observed that p53 acetylation is a reversible process and for it Mdm2 recruits HDAC1 (a histone deacetylase) to form a Mdm2-HDAC1 complex which deacetylates p53. Interestingly, it was also shown that p300 can form a complex with Mdm2 in vitro and in vivo [9,10] and this complex (Mdm2-p300) facilitate Mdm2 mediated p53 degradation. Moreover, it has also been reported that Mdm2-p53-p300 complex exists that is also thought to promote ubiquitylation and degradation of p53 [11]. Thus p300 plays dual role and exerts two opposite effects on p53 in cells i.e., it can either interact with Mdm2 promoting Mdm2-mediated ubiquitylation and degradation of p53 [9] or acetylate and stabilize p53. This remains puzzling.

There have been different mathematical techniques to study cellular and sub-cellular processes such as deterministic and stochastic models [12,13]. Stochastic model provide detail picture of molecular interaction in the microscopic systems (small systems with small number of molecules accomodated in each system) that leads the system dynamics as noise-driven process [13,14]. The model further highlights the important role of noise in the system

dynamics, for example detection and amplification of weak noise, the phenomenon known as stochastic resonance [15,16], lifting of cellular expression at different distinct expression state [17] and noise in gene expression can drive stochastic switching among such states [18,19], noise induced stochastic phenotypic switching to different new level in living cells [20] etc. However, deterministic model provides qualitative picture of the cellular or sub-cellular processes.

The aim of the present study is (i) to understand some of the basic issues of p53 autoregulation induced by regulators p300 and HDAC1, (ii) to elucidate the functional relationship of p300 and HDAC1 in regulating p53 function, (iii) how do these regulators lifts the normal p53-Mdm2 network to different stress states and (iv) what could be the role of noise in such situations.

Materials and Methods

Stress $p53-Mdm2$ model regulated by $p300$ and $HDAC1$

In normal proliferating cells, p53 is usually maintained at low levels due to p53 and Mdm2 protein feedback mechanism [21]. In unstressed condition the p53 binds to the regulatory region of Mdm2 gene and stimulates its transcription into messenger RNA (mRNA) with a transcription rate constant k_3, followed by translation into Mdm2 protein with a rate constant k_2 [22]. The degradation of Mdm2-mRNA, Mdm2 and genesis of p53 occurs with basal rate of k_4, k_5 and k_6 respectively. The Mdm2 protein then interacts physically with p53 to form Mdm2-p53 complex with the rate of k_8. Mdm2 functions as an E3 ubiquitin ligase and brings about ubiquitylation of multiple lysine residues (K370, K372, K373, K381, K382 and K386) [23] present in the C-terminal domain of p53 [11]. The ubiquitylation marks p53 for degradation via the 26S proteasome, with rate k_7. The Mdm2-p53 complex can also dissociate to Mdm2 and p53 with rate constant k_9. Mdm2 and p300 have been shown to interact with rate constant k_{20} to form Mdm2-p300 complex, which facilitates p53 polyubiquitination and degradation at rate constant of k_1 [9,24]. Although there is no direct evidence reported to the best of author's knowledge in the literature for the degradation of Mdm2-p300 complex, however it has been shown that the p19ARF-binding domain of Mdm2 overlaps with its p300-binding domain suggesting that p19ARF could interfere with the Mdm2/p300 interaction [9]. Therefore, we can assume it is possible that Mdm2-p300 complex can be broken so as to interact with other proteins. Thus in normal unstressed cell, p53 is maintained at low level in an active state with short half-life of 15–30 minutes by Mdm2 and the cells are able to proliferate.

However, under stressed conditions the p53 is stabilized through various post translational modifications which lead to increase its level. Of the various mechanisms, phosphorylation of $p53$ is the most well studied and it is reported that multiple kinases phosphorylate various residues which increase the level of $p53$ protein. One of these protein kinases is ATM which upon activation by DNA damage phosphorylates $p53$ with a rate k_{12} at serine 15 [25] which is critical for $p53$ activation and stabilization. Strikingly, the phosphorylation of serine 15 mediated by ATM acts as a nucleation event that promotes subsequent sequential modification of many residues. To achieve this, interconversion of inactivated and activated ATM takes place, with rate constants k_{10} and k_{11} respectively. The ATM-initiated phosphorylation reduces the affinity of $p53$ for $Mdm2$ while increases interactions with HATs like $CBP/p300$ [8,26]. Consequently, dephosphorylation of $p53$ with a rate k_{13} also takes place to counter this phosphorylation. It has been demonstrated that $p300$ protein is a co-activator of $p53$ which potentiates its transcriptional activity as well as biological function in vivo [27]. However, it has also been shown that formation of $p300\_Mdm2\_p53$ ternary complex leads to suppressing $p53$ acetylation and activation [28]. The transcription activation domain (TAD) of $p53$ binds tightly to $p300$ with formation rate constant k_{15}. The $p53\_p300$ complex hence formed, causes $p53$ acetylation with rate constant k_{16} at multiple lysine residues (K370, K372, K373, K381, K382) of its C-terminal regulatory domain [27,29]. The lysine residues (K370, K372, K373, K381, and K382) are the common sites for both acetylation and ubiquitination [30,31]. Thus their acetylation causes the inhibition of ubiquitination resulting $p53$ protein stability which is evident from the observation that acetylated $p53$ has half-life of greater than two hours [32]. Simultaneously, formation and degradation of $p300$ occurs with rate constants k_{23} and k_{14} respectively. $Mdm2$, $p53$ and $p300$ have also been demonstrated to exist in a ternary complex (k_{19}) which is incapable of acetylating $p53$ [28]. In the complex, TAD1 domain of $p53$ interacts with $Mdm2$ while TAD2 interacts with $p300$ [11]. As mentioned earlier, phosphorylation increases the affinity of $p53$ towards $p300$ while decreasing its affinity towards $Mdm2$. After phosphorylation, the ternary complex dissociates, with rate constant k_{21} into $Mdm2$ and $p53-p300$ complex, in which both TAD1 and TAD2 of $p53$ interact with $p300$ [11]. p300 can then acetylate and stabilize $p53$. Stabilized $p53$ functions as a tumor suppressor and induces high levels of $Mdm2$, which in turn promotes $p53$ degradation by recruiting a $p53$ deacetylase, $HDAC1$ with rate constant k_{24}. $HDAC1$ binds $Mdm2$ in a $p53$ dependent manner with binding rate constant k_{18} and deacetylates $p53$ with rate constant k_{17} at all known acetylated lysines in vivo [33]. Moreover, analysis has indicated the presence of MDM2, SMAR1 and HDAC1 complex under conditions of inhibited translation only 12 h post damage rescue while there is lack of complex formation 24 h post damage rescue, thereby suggesting degradation of the Mdm2-HDAC1complex [34]. HDAC1 is generated and degraded in cells with rate constants k_{24} and k_{22} respectively. The unmodified lysine residues can then serve as the substrates for $Mdm2$-mediated ubiquitylation resulting in $p53$ degradation and thus completing the feedback loop. The molecular species involved in the biochemical network are listed in Table 1 and the chemical reaction channels in the network are shown in Table 2. The schematic picture of the stress $p53-Mdm2$ autoregulatory biochemical reaction network model via $p300$ and $HDAC1$ based on the experimental evidences and reports mentioned above is shown in Fig. 1.

Stochastic description of biochemical reaction network

We now consider a configurational state $\vec{X}(t)=(X_1,X_2,\ldots,X_N)^T$ of the system of size V at any instant of time t defined by N molecular species undergoing M elementary reactions. The change in configurational state during any interval of time $[t,t+\Delta t]$ is due to random interaction of the participating molecules that leads to decay and creation of specific molecular species in state vector $\vec{X}(t)$ during the time interval [13,14,35]. Therefore the trajectory of this state vector $\vec{X}(t)$ as a function of time in the configurational space follows Markov process [13,14] and the dynamics of this vector becomes noise-induced stochastic process [13]. If we define $P(\vec{X},t)$ as the configurational probability of obtaining the state $\vec{X}$ at time t, then the time evolution of $P(\vec{X},t)$ will obey Master equation [13,14,36]. Even though the Master equation for complex system could be very difficult to solve analytically, different algorithms have been devised to solve the system dynamics numerically depending on

Table 1. List of molecular species.

S.No.	Species Name	Description	Notation
1.	$p53$	Unbounded $p53$ protein	x_1
2.	$Mdm2$	Unbounded $Mdm2$ protein	x_2
3.	$Mdm2\_mRNA$	$Mdm2$ messenger $mRNA$	x_3
4.	$Mdm2\_p53$	$Mdm2$ with $p53$ complex	x_4
5.	ATM_I	Inactivated ATM protein	x_5
6.	ATM_A	Activated ATM protein	x_6
7.	$p53\_P$	Phosphorylated $p53$ protein	x_7
8.	$p300$	Unbounded $p300$ protein	x_8
9.	$p53\_p300\_P$	Phosphorylated $p53\_p300$ complex	x_9
10.	$p53\_A$	Acetylated $p53$ protein (capped p53)	x_{10}
11.	$HDAC1$	Unbounded $HDAC1$ protein	x_{11}
12.	$Mdm2\_HDAC1$	$Mdm2$ and $HDAC1$ complex	x_{12}
13.	$Mdm2\_p53\_p300$	$Mdm2$, $p53$ and $p300$ complex	x_{13}
14.	$Mdm2\_p300$	$Mdm2$ and $p300$ complex	x_{14}

doi:10.1371/journal.pone.0052736.t001

the nature of the system. For example, stochastic simulation algorithm (Gillespie algorithm) for reaction system without considering time delay [13], stochastic simulation algorithm for time delay reaction system [37,38], τ-leap algorithm which is approximated algorithm of stochastic simulation algorithm for very complex reaction network [39], hybrid algorithm for reaction networks consisting of both slow and fast reactions [40] etc.

The Master equation for the stochastic system can be approximated to simpler Chemical Langevin equations (CLE) based on two important realistic approximations applied on the the system [41]. This can be done by defining a function $F(\vec{X},\Delta t)$ which is the number of a particular reaction fired during the time interval $[t,t+\Delta t]$ with $\Delta t\rangle 0$ and applying the two approximations: first applying $lim_{\Delta t\to 0}F(\vec{X},\Delta t)$ which leads to the prophensity functions (ω) of the reactions fired remain constant during the time interval, and secondly applying $lim_{\Delta t\to\infty}F(\vec{X},\Delta t)$ condition which gives rise $\omega\tau\rangle\rangle 1$ [41]. These two conditions are true for large population size of each variables in state vector $\vec{X}$ which is valid for natural systems. These two conditions allow the function F to approximate to Poisson distribution function and then to Normal distribution function with same mean and standard deviation. If molecular concentration is defined by $\{\vec{x}\}=\frac{1}{V}\{\vec{X}\}$ and linearize Normal distribution function, the Master equation leads to the following CLE of the vector $\vec{x}(t)$,

$$\frac{d\vec{x}(t)}{dt}=G[\omega(\vec{x}(t),v]+H[\omega(\vec{x}(t),v,\xi,V) \tag{1}$$

where, $G=\sum_{i=1}^{M}v_{ij}\omega_i[x(t)]$ is the macroscopic contribution term and $H=\frac{1}{\sqrt{V}}\sum_{i=1}^{M}v_{ij}[\omega_i\{x(t)\}]^{1/2}$ is the stochastic contribution term to the dynamics. $\xi_i = lim_{dt\to 0}N_i(0,1)/\sqrt{dt}$ is uncorrelated, statistically independent random noise parameters which satisfy $\xi_i(t)\xi_j(t') = \delta_{ij}\delta(t-t')$. $\{v\}$ is the stoichiometric matrix of the reactions in the network.

The classical deterministic equations can be obtained from the CLE equation (1) at thermodynamics limit [41] i.e. at $V\to\infty$, $N\to\infty$ but $N/V=constant$. This leads to $H\to 0$ and the equation (1) becomes noise free deterministic equation,

$$\frac{d\vec{x}(t)}{dt}=G[\omega(\vec{x}(t),v] \tag{2}$$

The same equation (2) can also be be retrieved from the biochemical reaction network by translating them into a set of differential equations based on standard principles of Mass-action law of biochemical reaction kinetics.

The stress $p53-Mdm2-p300-HDAC1$ model network we study is defined by $N=14$ (14 molecular species) and $M=24$ (24 reaction channels). The molecular species, possible reactions, kinetic laws and the rate constants in this model are listed in Table 1 and Table 2 respectively. The state vector at any instant of time t is given by, $\vec{x}(t)=(x_1,\ldots,x_{14})^T$, where the variables in the vector are various proteins and their complexes which are listed in Table 1. The classical deterministic equations constructed from these reaction network are given by,

$$\begin{aligned}\frac{dx_1}{dt}&=-k_1x_1x_{14}+k_6-k_8x_1x_2+k_9x_4\\&\quad-k_{12}x_1x_6+k_{13}x_7+k_{17}x_{10}x_{12}\end{aligned} \tag{3}$$

$$\begin{aligned}\frac{dx_2}{dt}&=k_2x_3-k_5x_2+k_7x_4-k_8x_1x_2\\&\quad+k_9x_4-k_{18}x_2x_{11}-k_{20}x_2x_8+k_{21}x_{13}\end{aligned} \tag{4}$$

$$\frac{dx_3}{dt}=k_3x_1-k_4x_3 \tag{5}$$

$$\frac{dx_4}{dt}=-k_7x_4+k_8x_1x_2-k_9x_4-k_{19}x_4x_8 \tag{6}$$

$$\frac{dx_5}{dt}=-k_{10}x_5+k_{11}x_6 \tag{7}$$

$$\frac{dx_6}{dt}=k_{10}x_5-k_{11}x_6-k_{12}x_1x_6 \tag{8}$$

$$\frac{dx_7}{dt}=k_{12}x_1x_6-k_{13}x_7-k_{15}x_7x_8 \tag{9}$$

$$\frac{dx_8}{dt}=-k_{14}x_8-k_{15}x_8x_7-k_{19}x_4x_8-k_{20}x_2x_8+k_{23} \tag{10}$$

$$\frac{dx_9}{dt}=k_{15}x_8x_7-k_{16}x_9+k_{21}x_{13} \tag{11}$$

Table 2. List of chemical reaction, propensity function and their rate constant.

S.No	Reaction	Name of the process	Kinetic law	Rate constant	References
1	$x_1 + x_{14} \xrightarrow{k_1} \phi$	p53 degradation	$k_1\langle x_1\rangle\langle x_{14}\rangle$	$8.25\times10^{-4}sec^{-1}$	[9,24].
2	$x_3 \xrightarrow{k_2} x_3 + x_2$	Mdm2 creation	$k_2\langle x_3\rangle$	$4.95\times10^{-4}sec^{-1}$	[22].
3	$x_1 \xrightarrow{k_3} x_1 + x_3$	$Mdm2\_mRNA$ creation	$k_3\langle x_1\rangle$	$1.0\times10^{-4}sec^{-1}$	[22].
4	$x_3 \xrightarrow{k_4} \phi$	$Mdm2\_mRNA$ degradation	$k_4\langle x_3\rangle$	$1.0\times10^{-4}sec^{-1}$	[22].
5	$x_2 \xrightarrow{k_5} \phi$	Mdm2 degradation	$k_5\langle x_2\rangle$	$4.33\times10^{-4}sec^{-1}$	[22].
6	$\phi \xrightarrow{k_6} x_1$	p53 synthesis	k_6	$0.078sec^{-1}$	[22].
7	$x_4 \xrightarrow{k_7} x_2$	$Mdm2\_p53$ degradation	$k_7\langle x_4\rangle$	$8.25\times10^{-4}sec^{-1}$	[11,23].
8	$x_1 + x_2 \xrightarrow{k_8} x_4$	$Mdm2\_p53$ synthesis	$k_8\langle x_1\rangle\langle x_2\rangle$	$11.55\times10^{-4}sec^{-1}$	[22].
9	$x_4 \xrightarrow{k_9} x_1 + x_2$	$Mdm2\_p53$ dissociation	$k_9\langle x_4\rangle$	$11.55\times10^{-6}sec^{-1}$	[22].
10	$x_5 \xrightarrow{k_{10}} x_6$	ATM activation	$k_{10}\langle x_5\rangle$	$1.0\times10^{-4}sec^{-1}$	[12,23].
11	$x_6 \xrightarrow{k_{11}} x_5$	ATM deactivation	$k_{11}\langle x_6\rangle$	$5.0\times10^{-4}sec^{-1}$	[12,23].
12	$x_1 + x_6 \xrightarrow{k_{12}} x_6 + x_7$	Phosphorylation of p53	$k_{12}\langle x_1\rangle\langle x_6\rangle$	$5.0\times10^{-4}sec^{-1}$	[23].
13	$x_7 \xrightarrow{k_{13}} x_1$	Dephosphorylation of p53	$k_{13}\langle x_7\rangle$	$5.0\times10^{-1}sec^{-1}$	[12,23].
14	$x_8 \xrightarrow{k_{14}} \phi$	p300 degradation	$k_{14}\langle x_8\rangle$	$1.0\times10^{-4}sec^{-1}$	[30,31].
15	$x_7 + x_8 \xrightarrow{k_{15}} x_9$	$p53\_p300formation$	$k_{15}\langle x_7\rangle\langle x_8\rangle$	$1.0\times10^{-4}sec^{-1}$	[28].
16	$x_9 \xrightarrow{k_{16}} x_{10}$	Acetylation of p53	$k_{16}\langle x_9\rangle$	$1.0\times10^{-4}sec^{-1}$	[27,29].
17	$x_{10} + x_{12} \xrightarrow{k_{17}} x_1$	Deacetylation of p53	$k_{17}\langle x_{10}\rangle\langle x_{12}\rangle$	$1.0\times10^{-5}sec^{-1}$	[29].
18	$x_2 + x_{11} \xrightarrow{k_{18}} x_{12}$	Creation of $Mdm2\_HDAC1$	$k_{18}\langle x_2\rangle\langle x_{11}\rangle$	$2.0\times10^{-4}sec^{-1}$	[29].
19	$x_4 + x_8 \xrightarrow{k_{19}} x_{13}$	Creation of $Mdm2\_p53\_p300$	$k_{19}\langle x_4\rangle\langle x_8\rangle$	$5.0\times10^{-4}sec^{-1}$	[28].
20	$x_2 + x_8 \xrightarrow{k_{20}} x_{14}$	Formation of $Mdm2\_p300$	$k_{20}\langle x_2\rangle\langle x_8\rangle$	$5.0\times10^{-4}sec^{-1}$	[9,22].
21	$x_{13} \xrightarrow{k_{21}} x_4 + x_8$	Dissociation of $Mdm2\_p53\_p300$	$k_{21}\langle x_{13}\rangle$	$1.0\times10^{-4}sec^{-1}$	[11,28].
22	$x_{11} \xrightarrow{k_{22}} \phi$	Degradation of HDAC1	$k_{22}\langle x_{11}\rangle$	$1.0\times10^{-4}sec^{-1}$	[29].
23	$\phi \xrightarrow{k_{23}} x_8$	p300 synthesis	$k_{23}(k_{p300})$	$0.08sec^{-1}$	[30,31].
24	$\phi \xrightarrow{k_{24}} x_{11}$	HDAC1 synthesis	$k_{24}(k_{HDAC1})$	$2.0\times10^{-4}sec^{-1}$	[29].

doi:10.1371/journal.pone.0052736.t002

$$\frac{dx_{10}}{dt} = k_{16}x_9 - k_{17}x_{10}x_{12} \tag{12}$$

$$\frac{dx_{11}}{dt} = -k_{18}x_2x_{11} - k_{22}x_{11} + k_{24} \tag{13}$$

$$\frac{dx_{12}}{dt} = -k_{17}x_{10}x_{12} + k_{18}x_2x_{11} \tag{14}$$

$$\frac{dx_{13}}{dt} = k_{19}x_4x_8 - k_{21}x_{13} \tag{15}$$

$$\frac{dx_{14}}{dt} = -k_1x_1x_{14} + k_{20}x_2x_8 \tag{16}$$

where, $\{k_i\}$ and $\{x_i\}$, $i=1,2,\ldots,N(N=14)$ represent the sets of rate constants of the reactions listed in Table 2 and concentrations of the molecular populations listed in Table 1.

Following the same procedure as we have discussed above, we reach the following CLE for the network shown in Fig. 1, Table 1 and Table 2.

$$\begin{aligned}\frac{dx_1}{dt} &= -k_1x_1x_{14} + k_6 - k_8x_1x_2 + k_9x_4 - k_{12}x_1x_6 \\ &+ k_{13}x_7 + k_{17}x_{10}x_{12} + \frac{1}{\sqrt{V}}\left[-\sqrt{k_1x_1x_{14}}\xi_1\right] + \frac{1}{\sqrt{V}} \\ &\left[\sqrt{k_6}\xi_2 - \sqrt{k_8x_1x_2}\xi_3 + \sqrt{k_9x_4}\xi_4 - \sqrt{k_{12}x_1x_6}\xi_5 + \sqrt{k_{13}x_7}\xi_6 + \sqrt{k_{17}x_{10}x_{12}}\xi_7\right]\end{aligned} \tag{17}$$

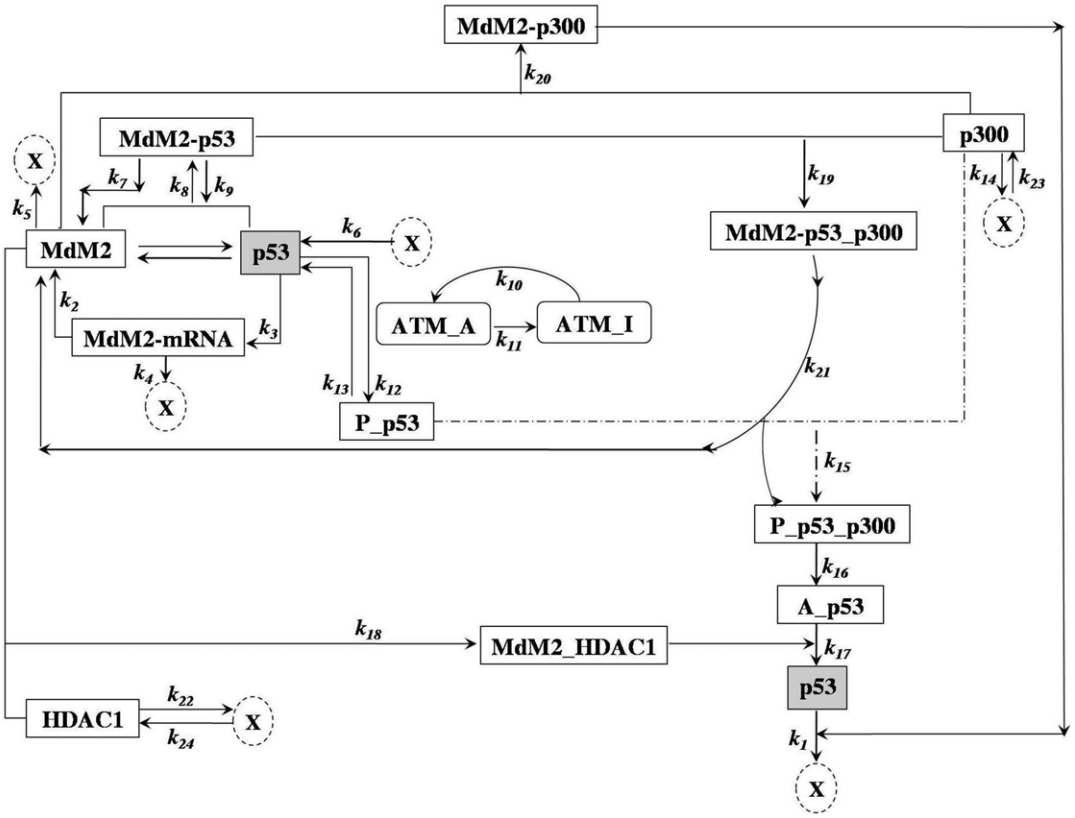

Figure 1. Biochemical network model of stress p53-Mdm2-p300-HDAC1. The schematic diagram of stress p53-Mdm2-p300-HDAC1 model.
doi:10.1371/journal.pone.0052736.g001

$$\frac{dx_2}{dt} = k_2x_3 - k_5x_2 + k_7x_4 - k_8x_1x_2 + k_9x_4 - k_{18}x_2x_{11} - k_{20}x_2x_8 + k_{21}x_{13} + \frac{1}{\sqrt{V}}\left[\sqrt{k_2x_3}\xi_8 - \sqrt{k_5x_2}\xi_9 + \sqrt{k_7x_4}\xi_{10} - \sqrt{k_8x_1x_2}\xi_{11} + \sqrt{k_9x_4}\xi_{12}\right] + \frac{1}{\sqrt{V}}\left[-\sqrt{k_{18}x_2x_{11}}\xi_{13} - \sqrt{k_{20}x_2x_8}\xi_{14} - \sqrt{k_{21}x_{13}}\xi_{15}\right] \quad (18)$$

$$\frac{dx_3}{dt} = k_3x_1 - k_4x_3 + \frac{1}{\sqrt{V}}\left[\sqrt{k_3x_1}\xi_{16} - \sqrt{k_4x_3}\xi_{17}\right] \quad (19)$$

$$\frac{dx_4}{dt} = -k_7x_4 + k_8x_1x_2 - k_9x_4 - k_{19}x_4x_8 + \frac{1}{\sqrt{V}}\left[-\sqrt{k_7x_4}\xi_{18} + \sqrt{k_8x_1x_2}\xi_{19} - \sqrt{k_9x_4}\xi_{20} - \sqrt{k_{19}x_4x_8}\xi_{21}\right] \quad (20)$$

$$\frac{dx_5}{dt} = -k_{10}x_5 + k_{11}x_6 + \frac{1}{\sqrt{V}}\left[-\sqrt{k_{10}x_5}\xi_{22} + \sqrt{k_{11}x_6}\xi_{23}\right] \quad (21)$$

$$\frac{dx_6}{dt} = k_{10}x_5 - k_{11}x_6 - k_{12}x_1x_6 + \frac{1}{\sqrt{V}}\left[\sqrt{k_{10}x_5}\xi_{24} - \sqrt{k_{11}x_6}\xi_{25} - \sqrt{k_{12}x_1x_6}\xi_{26}\right] \quad (22)$$

$$\frac{dx_7}{dt} = k_{12}x_1x_6 - k_{13}x_7 - k_{15}x_7x_8 + \frac{1}{\sqrt{V}}\left[\sqrt{k_{12}x_1x_6}\xi_{27} - \sqrt{k_{13}x_7}\xi_{28} - \sqrt{k_{15}x_7x_8}]\xi_{29}\right] \quad (23)$$

$$\frac{dx_8}{dt} = -k_{14}x_8 - k15x_8x_7 - k_{19}x_4x_8 - k_{20}x_2x_8 + k_{23} + \frac{1}{\sqrt{V}}\left[-\sqrt{k_{14}x_8}\xi_{30} - \sqrt{k_{15}x_8x_7}\xi_{31} - \sqrt{k_{19}x_4x_8}\xi_{32} - \sqrt{k_{20}x_2x_8}\xi_{33} - \sqrt{k_{23}}\xi_{34}\right] \quad (24)$$

$$\frac{dx_9}{dt} = k_{15}x_8x_7 - k_{16}x_9 + k_{21}x_{13} + \frac{1}{\sqrt{V}}\left[\sqrt{k_{15}x_8x_7}\xi_{35} - \sqrt{k_{16}x_9}\xi_{36} - \sqrt{k_{21}x_{13}}\xi_{37}\right] \quad (25)$$

$$\frac{dx_{10}}{dt} = k_{16}x_9 - k_{17}x_{10}x_{12} + \frac{1}{\sqrt{V}}\left[\sqrt{k_{16}x_9}\xi_{38} - \sqrt{k_{17}x_{10}x_{12}}\xi_{39}\right] \quad (26)$$

$$\frac{dx_{11}}{dt} = -k_{18}x_2x_{11} - k_{22}x_{11} + k_{24} + \frac{1}{\sqrt{V}}\left[\sqrt{k_{18}x_2x_{11}}\xi_{40} - \sqrt{k_{22}x_{11}}\xi_{41} + \sqrt{k_{24}}\xi_{42}\right] \quad (27)$$

$$\frac{dx_{12}}{dt} = -k_{17}x_{10}x_{12} + k_{18}x_2x_{11} + \frac{1}{\sqrt{V}}\left[-\sqrt{k_{17}x_{10}x_{12}}\xi_{43} + \sqrt{k_{18}x_2x_{11}}\xi_{44}\right] \quad (28)$$

$$\frac{dx_{13}}{dt} = k_{19}x_4x_8 - k_{21}x_{13} + \frac{1}{\sqrt{V}}\left[\sqrt{k_{19}x_4x_8}\xi_{45} - \sqrt{k_{21}x_{13}}\xi_{46}\right] \quad (29)$$

$$\frac{dx_{14}}{dt} = -k_1x_1x_{14} + k_{20}x_2x_8 + \frac{1}{\sqrt{V}}\left[-\sqrt{k_1x_1x_{14}}\xi_{47} + \sqrt{k_{20}x_2x_8}\xi_{48}\right] \quad (30)$$

where, $\{\xi_i\}$ are random number which satisfy $\xi_i(t)\xi_j(t') = \delta_{ij}\delta(t-t')$, and V is the system's size.

The CLE (3)-(17) and differential equations (18)-(32) can be solved numerically using standard algorithm of 4th order Runge-Kutta method of numerical integration [42].

Results and Discussion

Several researchers have studied the oscillations of $p53-Mdm2$ network in detail [22,43–46], however to the best of our knowledge this study is the first one that uses systems biology approach for understanding the complex role of p300 and HDAC1 on p53. We numerically solved the set of deterministic differential equations (1)–(14), and stochastic CLE (15)–(29) by using standard algorithm of 4th order Runge-Kutta method of numerical integration [42]. We thus study the impact of p300 and HDAC1 on p53 activation and stabilization to understand the fate of the cell.

Impact of $p300$ on $p53-Mdm2$ activation

We first present the deterministic results on p53-Mdm2 regulatory network on exposure to different concentrations of $p300$ i.e. at different rate constants, k_{p300} (Fig. 2). For small values of k_{p300} ($=0.04$) (lower $p300$ concentration), $p53$ is first activated for some time ($\sim 30 hours$) and then resumes its normal condition indicated by its constant level (~ 12.4) which is the level of stabilization. The range of activation is increased as k_{p300} increases (increase of $p300$ concentration) as well as there is rise in the level of stabilization. However, when $k_{p300} = 0.06-0.08$, $p53$ maintains sustain oscillations which leads to increasing level of activation as a consequence. With further increment of $p300$ concentration level, $p53$ dynamics that was at sustain oscillations switched to damped oscillations and subsequently p53 concentration is stabilized at a constant level. This activity suggests that the capping of the c-terminal of $p53$ is higher and there is no decrement in the $p53$ levels as a result of which $p53$ is stabilized. The results obtained are consistent with the experimental observations which indicates that acetylation of p53 is responsible for its activation [27,31] and stabilization [29,32]. If we further increase the value of k_{p300}, $p53$ activation decreases maintaining $p53$ stability but at higher values (≥ 80). Hence we identify two conditions where p53 is stabilized, one at lower values (nearly normal cell condition) and the other at larger values (cell death condition) of k_{p300} and in between $p53$ is activated.

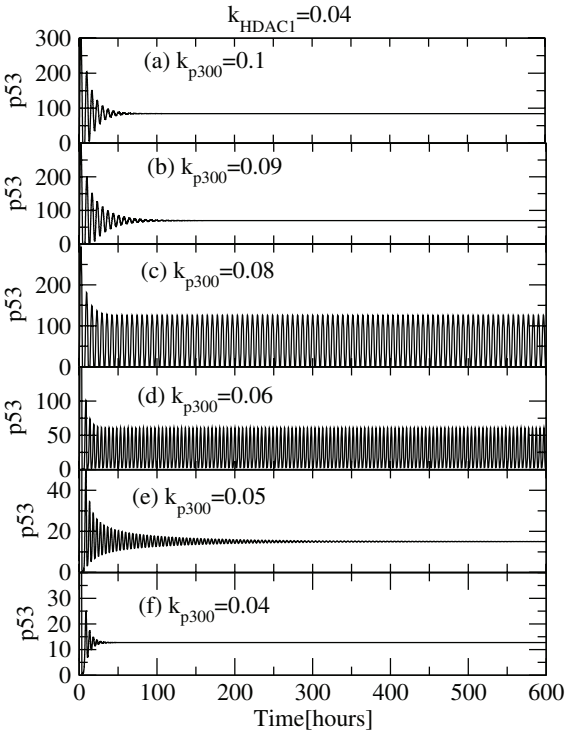

Figure 2. $p53$ dynamics for various $p300$ levels. The plots of $p53$ concentration levels as a function of time in hours for various k_{p300} values: (a) $k_{p300}=0.1$, (b) $k_{p300}=0.09$, (c) $k_{p300}=0.08$, (d) $k_{p300}=0.06$, (e) $k_{p300}=0.05$ and (f) $k_{p300}=0.04$ respectively at constant value of $k_{HDAC1}=0.04$.
doi:10.1371/journal.pone.0052736.g002

Similarly, $Mdm2$ dynamics as a function of time for different values of $p300$ concentration levels is shown (Fig. 3) that demonstrates counter behaviour as expected. The two dimensional recurrence plots of ($p53-Mdm2$), ($p53-p300$) and ($Mdm2-p300$) are presented in Fig. 4 which provides clear and qualitative picture of the above facts. The emergence of sustain/limit-cycle oscillation (activated $p53$ level) from fix point oscillation (stabilized $p53$ level), and then from sustain oscillation to again fix point oscillation is observed as one increase the concentration of $p300$.

Impact of $HDAC1$ on $p53-Mdm2$ network

Several studies suggest that $HDAC1$ is involved in the deacetylation of p53 which has a potent impact on $p53-Mdm2$ regulatory dynamics [29,31,47,48]. It has been found that $HDAC1$ makes complex protein, $HDAC1-Mdm2$ which

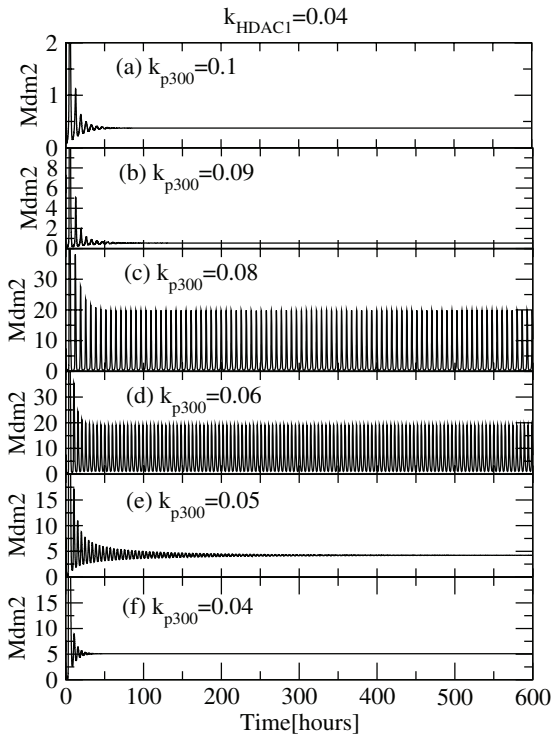

Figure 3. *Mdm2* dynamics for various *p300* levels. The plots of *Mdm2* concentration levels as a function of time in hours for various k_{p300} values: (a) $k_{p300}=0.1$, (b) $k_{p300}=0.09$, (c) $k_{p300}=0.08$, (d) $k_{p300}=0.06$, (e) $k_{p300}=0.05$ and (f) $k_{p300}=0.04$ respectively at constant value of $k_{HDAC1}=0.04$.
doi:10.1371/journal.pone.0052736.g003

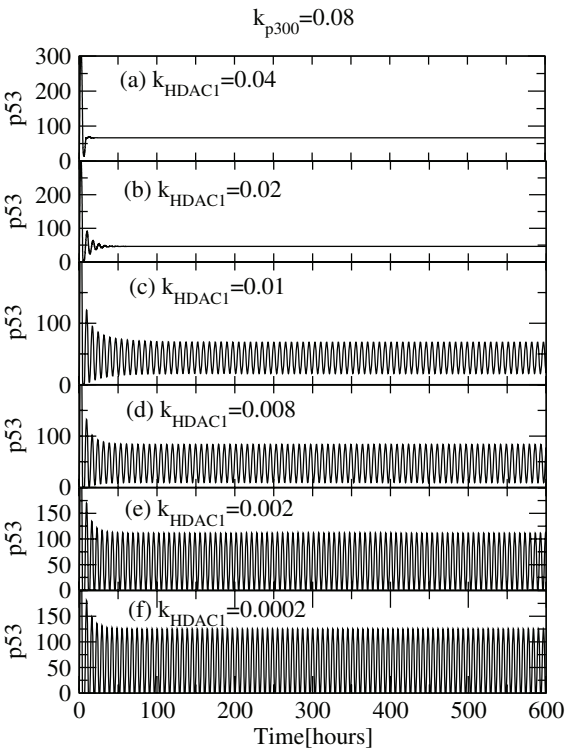

Figure 5. Activation of *p53* via variation of *HDAC1* level. Plots of *p53* concentration levels as a function of time in hours for various k_{HDAC1} values 0.0002, 0.002, 0.008, 0.01, 0.02 and 0.04 respectively (at constant value of $k_{p300}=0.08$), showing activation and stabilization of *p53*.
doi:10.1371/journal.pone.0052736.g005

deacetylates and then ubiquitinates the acetylated *p53*. Because of this process of interaction of *HDAC1* with *p53*, both *p53* and *Mdm2* levels get stabilized. In our numerical simulation, we kept *p300* concentration level fixed by keeping $k_{p300}=0.08$ throughout the simulation and allow *HDAC1* concentration to vary by changing k_{HDAC1} value. The results are shown in Fig. 5 (a)–(f). In these plots we observe that at lower concentration of *HDAC1* ($k_{HDAC1}=0.0002$), the *p53* activation is large due to pre-existing *p300*, as indicated by the sustained oscillation (Fig. 5 (f)). This activity suggests that there is regular decay and creation of *p53*, due to the presence of high levels of *p300* and hence the impact of *HDAC1* concentration level is not very significant. As the *HDAC1* concentration increases (increasing k_{HDAC1} value), there is regular and competitive effect between *p300* and *HDAC1* for *p53* that decreases *p53* activation as indicated by decrease in *p53* concentration level (Fig. 5 (c)–(e)). Further, if we increase the

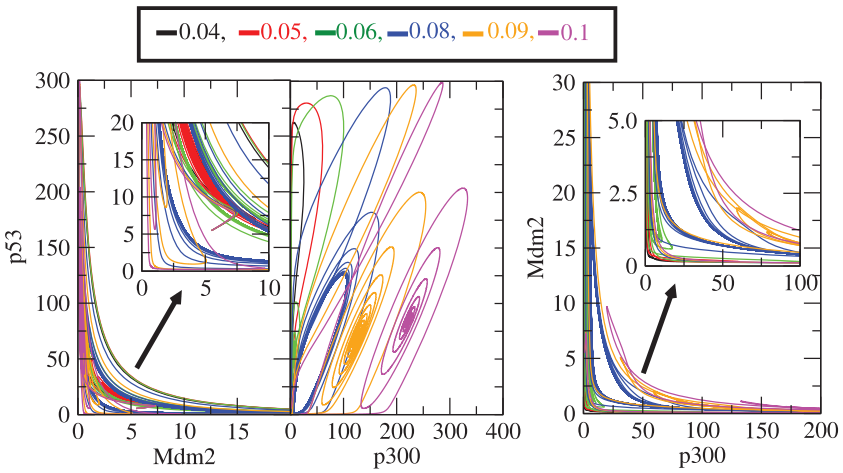

Figure 4. Two-dimensional recurrence plots of *p53* and *Mdm2*. Recurrence plots between ($p53-Mdm2$), ($p53-p300$) and ($Mdm2-p300$) for different values of rate constants k_{p300}, i.e. 0.04, 0.05, 0.06, 0.08, 0.09 and 0.1 respectively.
doi:10.1371/journal.pone.0052736.g004

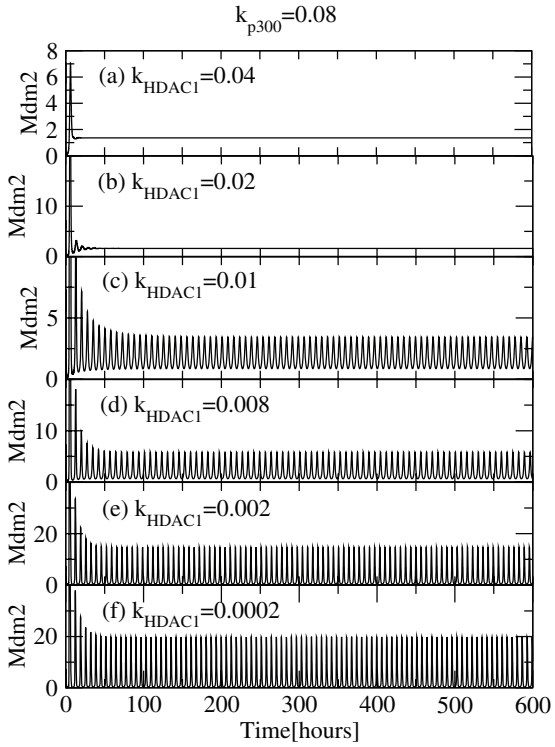

Figure 6. Activation of *Mdm2* via variation of *HDAC1* level. Plots of *Mdm2* concentration levels as a function of time in hours for various k_{p300} values 0.0002, 0.002, 0.008, 0.01, 0.02 and 0.04 respectively (at constant value of $k_{p300}=0.08$), showing activation and stabilization of *Mdm2*.
doi:10.1371/journal.pone.0052736.g006

concentration of *HDAC*1, the *p*53 first activates for short period of time and then remains constant at same value ($\sim$50) indicating *p*53 stabilization. This transition from *p*53 activation to stabilization is indicated by the transition from sustained oscillation to fixed point oscillations indicated in Fig. 5 (a) and (b). We observe this behaviour at $k_{HDAC1}=0.04$, where the activity of *p*53 is low, stable and very much controlled.

Similarly, we present the simulation results of *Mdm*2 as a function of time for different *HDAC*1 levels (Fig. 6 (a)–(f)). We observe similar behaviour of *Mdm*2 as *p*53 which shows a transition from sustain oscillation to fix point oscillation as one increase the *HDAC*1 concentration level. These results indicate that *HDAC*1 stabilizes *p*53 as well as *Mdm*2 concentration levels.

We also present the two dimensional recurrence plots of the (*p*53 – *Mdm*2), (*p*53 – *HDAC*1) and (*Mdm*2 – *HDAC*1) for demonstrating these facts (Fig. 7). The clear indication of transition from sustain/limit cycle oscillation to fix point oscillation as k_{HDAC1} is increased, is shown in the plots indicating transition from activation of *p*53 and *Mdm*2 to stabilized state.

Stability analysis of *p*53 and *Mdm*2

We then checked how concentration level of *p*53 varies as a function of k_{p300} ($\propto$concentration levels of *p*300). This is done by defining a parameter called expose time (η) which can be stated as the amount of time the system is exposed to a particular concentration level of *p*300 or *HDAC*1. The calculation of *p*53 or *Mdm*2 concentration level induced by the exposition of the system to *p*300 or *HDAC*1 is done by obtaining its level just after the expose time (time slice calculation). Fig. 8 shows variation of *p*53 concentration levels as a function of k_{p300} for different expose times of 10–100 hours for a fixed value of $k_{HDAC1}=0.04$. The plots clearly show the activated and stabilized regimes. The activated regime is where the *p*53 levels fluctuate as a function of k_{p300} (induced by *p*300 levels). In the plots, *p*53 level starts activation from $k_{p300}\sim0.27$ because of the interaction among *p*53, *Mdm*2 and *p*300 with small level of *HDAC*1 giving rise to fluctuation in *p*53 level. This could be due to acetylation and deacetylation which leads to capping (which prohibits *p*53 to decay) and uncapping (which leads to *p*53 decay) of *p*53 due to *p*300. This *p*53 level fluctuation persists till $k_{p300}\sim0.55$ and then increases its level without fluctuation till $k_{p300}\sim2.74$ indicating only the capping of *p*300, then its level remain constant. Interestingly the range of activation of k_{p300} in *p*53 for all expose times remain the same in [0.27–2.74].

The stabilized regimes are where *p*53 level is not affected by the variation in k_{p300} (*p*300 level variation). Initially, within the range of k_{p300} [0–0.27], the *p*53 level is not much affected indicating that the cell resumes its normal condition maintaining its minimum level ($\sim$13) which we call first stabilization regime. However, in

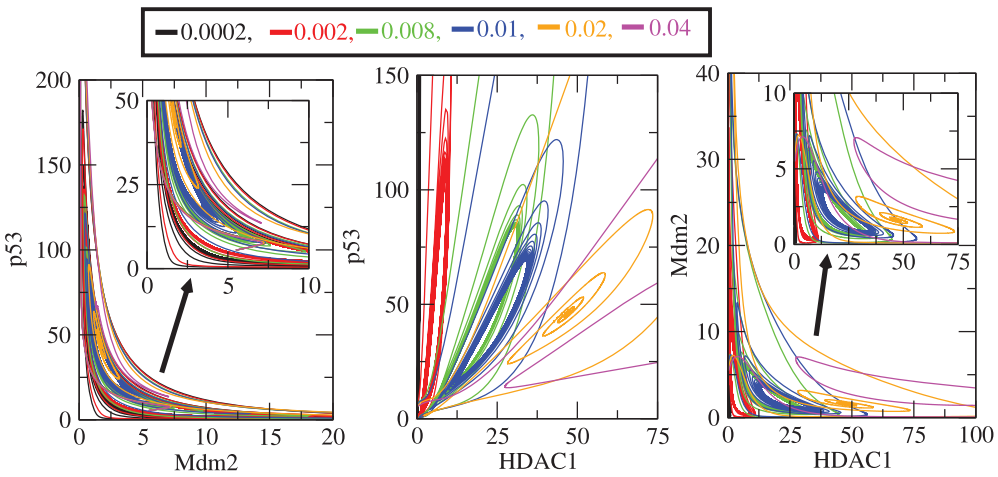

Figure 7. Recurrence plots of *p*53 and *Mdm*2 activated by *HDAC1*. The two dimensional plots of the pairs (*p*53 – *Mdm*2), (*p*53 – *HDAC*1) and (*Mdm*2 – *HDAC*1) for different values of rate constants k_{HDAC1}, i.e. 0.0002, 0.002, 0.08, 0.01, 0.02 and 0.04 respectively.
doi:10.1371/journal.pone.0052736.g007

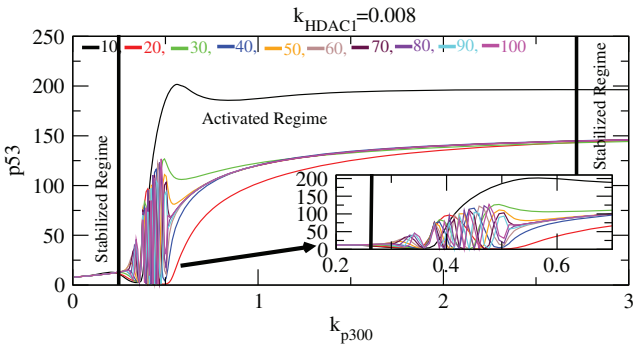

Figure 8. Stability curve induced by *p300*. Plots of $p53$ concentration level as a function of k_{300} for different values of exposure times i.e. $\eta = 10$-100 (at constant value of $k_{HDAC1} = 0.04$). The inset is the enlarged portion of the activated regime. In the curve stabilized and activated regimes are demarcated.
doi:10.1371/journal.pone.0052736.g008

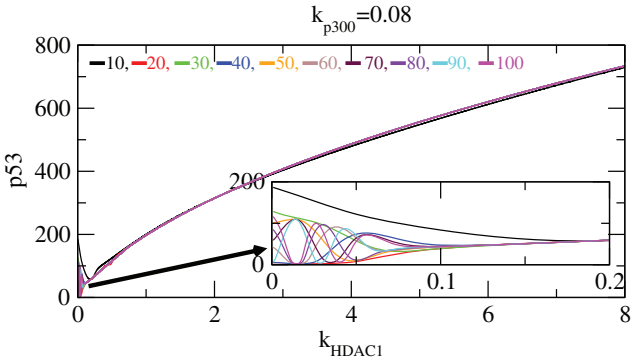

Figure 10. Stability curve induced by *HDAC1*. The variation of $p53$ concentration level versus k_{HDAC1} for different exposure times $\eta = 10$–100, keeping $k_{p300} = 0.08$ fixed. The inset is the enlarged portion of the actively activated regime.
doi:10.1371/journal.pone.0052736.g010

the second stabilization regime [2.74–∞], $p53$ level remains constant at much higher value ($\sim$145) indicating the capping of $p53$ is maximum utilizing $p300$ which prohibits decay. This case may be the condition where death of the cell could happen due to uncontrolled $p53$ growth due to excess $p300$.

The activation and stabilization of *Mdm2* induced by $p300$ is shown in Fig. 9. Since *Mdm2* is counter part of $p53$ which is activated by $p53$, similar results are obtained as in the case of $p53$. The first stabilization regime is within [0–0.23] values of k_{p300}, followed by activation regime [$\langle$0.23–0.7] and finally second stabilization regime [$\langle$0.7–∞]. The increased level of $p53$ in the second stabilization regime are capped $p53$ level which are prohibited from decay and taking part in any other reactions and therefore is not able to activate *Mdm2* level. Hence its level reduces to minimum as soon as the second stabilization regime is reached.

Next we study the impact of *HDAC1* on $p53$ stabilization in our system. This is done by keeping the value of k_{p300} fixed at 0.08 and simulating the level of $p53$ as a function of k_{HDAC1} for different exposure times 10–100 hours (Fig. 10). From the plots one can see the activation of $p53$ at low k_{HDAC1} values due to $p300$ impact but not due to *HDAC1* contribution. As k_{HDAC1} value increases, the $p53$ level starts decreasing due the deacetylation of $p53$ which allow it to degrade and take part in reactions. The activation of $p53$ with fluctuation persists till ($k_{HDAC1} \leq 0.1$). After ($k_{HDAC1} \rangle 0.1$), $p53$ level remains constant for a short period of time and then its level starts increasing without fluctuation. This behaviour indicates that *HDAC1* has suppressing impact on $p53$ activation. This pattern is same for all exposure times as is shown in the plots (Fig. 10). The same pattern is found for *Mdm2* also which in fact is the counterpart of $p53$. The activated and stabilized regimes are shown in the Fig. 11.

We then present the results of amplitudes of $p53$, (A_{p53}) and time period, (T_{p53}) as a function of k_{p300} and k_{HDAC1} to understand the how $p300$ and *HDAC1* influence the amplitude and time period of $p53$ oscillations (Fig. 12). The calculation of $p53$ amplitude is done as in the following. For sustain oscillation we took time range of [100–200] hours in our calculation and then calculated the average of it. Then we take 50 such time series for different initial conditions and determine the average of p53 amplitude again (Fig. 12 and 13). The points in the plots are average points with error bars. For damped oscillations, we take the available number of oscillations and calculated the average of those oscillations which is found to be equivalent to the distance between x-axis and line which shows no oscillation (stable line) approximately. Similarly, for stabilized regime we determine

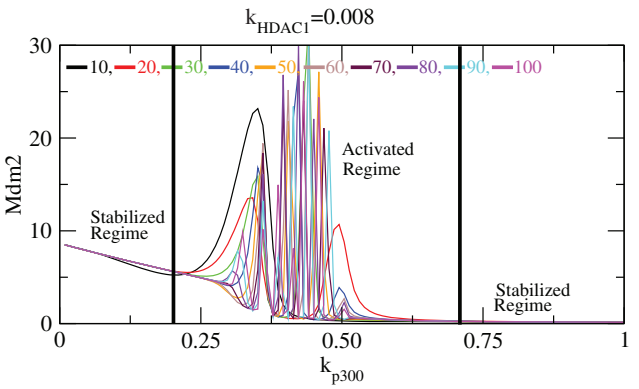

Figure 9. Stability curve induced by *p300*. Plots of *Mdm2* concentration level as a function of k_{300} for different values of exposure times i.e. $\eta = 10$–100 (at constant value of $k_{HDAC1} = 0.04$). In the curve stabilized and activated regimes are demarcated.
doi:10.1371/journal.pone.0052736.g009

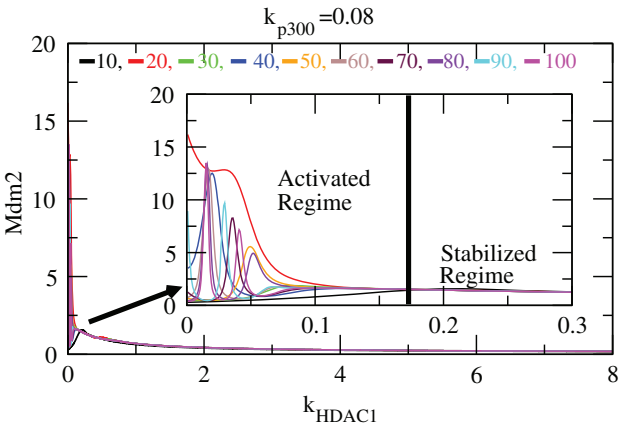

Figure 11. Stability curve induced by *HDAC1*. The variation of *Mdm2* concentration level versus k_{HDAC1} for different exposure times $\eta = 10$–100, keeping $k_{p300} = 0.08$ fixed. The inset is the enlarged portion of the activated and stabilized regimes.
doi:10.1371/journal.pone.0052736.g011

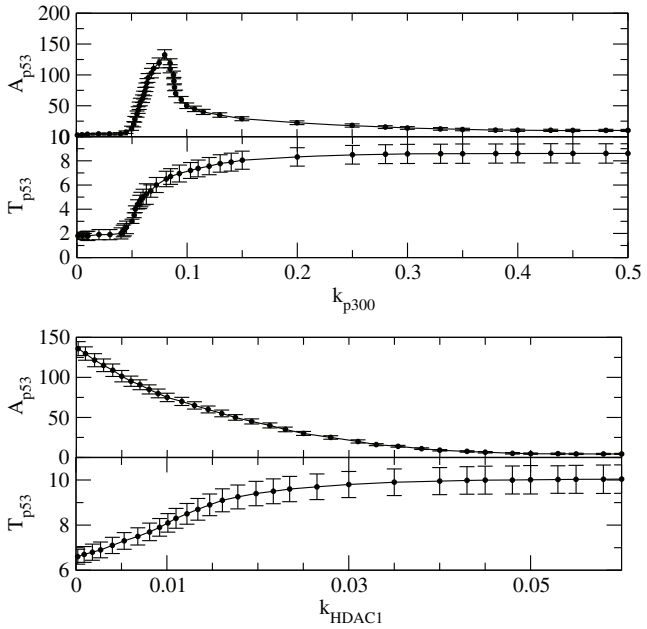

Figure 12. The variation of *p*53 amplitude and time period induced by *p*300. (a) Plots of A_{p53} and T_{p53} as a function of k_{p300} (upper two panels) which capture the stabilized and activated regimes. (b) Plots of A_{p53} and T_{p53} as a function of k_{HDAC1} (lower two panels) which capture the stabilized and activated regimes.
doi:10.1371/journal.pone.0052736.g012

distance between x-axis and stable line for each values of k_{p300} or k_{HDAC1} and average over 50 time series. Initially, A_{p53} remains constant at lowest value for small values [0–0.05] of k_{p300}, then it monotonically increases and decrease in the interval [0.05–0.3] and finally its value remains constant. This in fact is the consequence of first stability (normal condition) where the impact of $p300$ is negligible, then activation of $p53$ due to interaction of $p300$ with $p53$ and other proteins and then stabilization of $p53$. These three regimes can also be seen in the case of T_{p300} versus k_{300} plot.

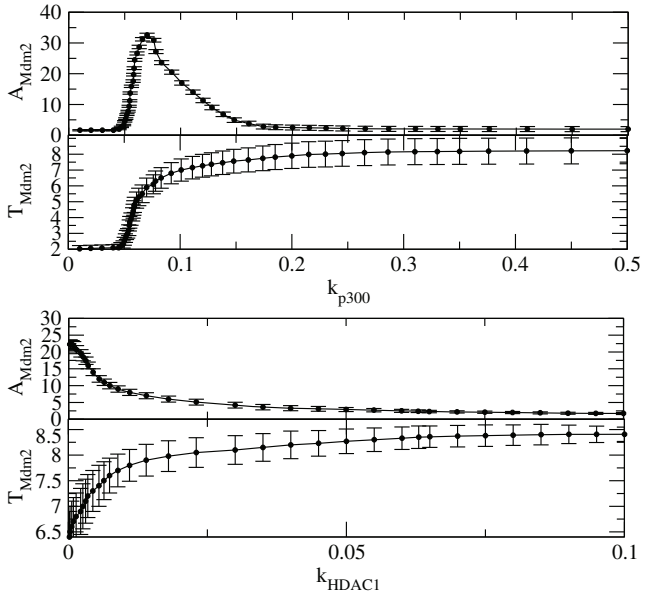

Figure 13. The variation of *Mdm*2 amplitude and time period induced by *HDAC1*. (a) Plots of A_{Mdm2} and T_{Mdm2} as a function of k_{p300} (upper two panels) which capture the stabilized and activated regimes. (b) Plots of A_{Mdm2} and T_{Mdm2} as a function of k_{HDAC1} (lower two panels) which capture the stabilized and activated regimes.
doi:10.1371/journal.pone.0052736.g013

However, in the case of A_{p53} and T_{p53} induced by $HDAC1$, the first stability condition is not observed because the cell is already activated with a constant $p300$ level i.e. at constant $k_{p300}=0.08$. In this case A_{p53} level decreases as k_{HDAC1} increases till $k_{HDAC1}=0.03$ and the remains constant. However, T_{p53} increases till $k_{HDAC1}=0.03$ and then stabilized.

Similarly we calculated A_{Mdm2} and T_{Mdm2} as a function of k_{300} and k_{HDAC1} respectively and the results are shown in Fig. 12. For both the parameters similar behaviour was obtained as in the case of $p53$.

Deterministic steady state solutions: impact of $HDAC1$ and $p300$ on $p53$

The steady state solutions in deterministic case can be obtained by putting the conditions $\frac{dx_i(t)}{dt}=0$, $i=1,2,\ldots,N$, where $N=14$, to the set of differential equations (3)–(16) and solving for various variables $\{x_i^*\}$. Following this procedure we first solve for x_1^{*d} (steady state solution of p53) as a function of x_{11}^* (steady state solution of HDAC1). The result is given by,

$$x_1^{*d}(x_{11}^*)\sim\Gamma\left(\alpha+\beta x_{11}^*+\frac{\gamma}{x_{11}^*}\right) \tag{31}$$

where, $\Gamma=\frac{k_4}{k_2k_3}$, $\alpha=k_{23}(1+\frac{k_{14}k_{18}}{k_{20}k_{22}})-\frac{k_{22}}{k_{18}}(k_5+\frac{k_{18}k_{24}}{k_{22}})$, $\beta=k_{18}(1+\frac{k_{22}}{k_{18}}+\frac{k_{14}}{k_{20}})$ and $\gamma=\frac{k_{24}}{k_{22}}(\frac{k_5k_{22}}{k_{18}}-\frac{k_{23}k_{18}k_{14}}{k_{22}k_{20}})$ are constants. The equation (31) shows that the increase in x_{11} leads to increase in x_1^{*d} and second term in the equation is the main contributer. The reason being as x_{11}^* increases the third term $\frac{\gamma}{x_{11}^*}\to 0$ and the first term is a constant. Further, increase in k_{22} (degradation rate of HDAC1) and k_{14} (degradation rate of p300) contribute increase in β, and therefore increases the steady state level of x_1^{*d}. From the expression of α, one can see that if $\frac{k_{23}}{k_{22}}>1$ (p300 synthesis rate is larger than HDAC1 degradation rate), α will contribute positive to x_1^{*d}, otherwise it will give negative contribution.

Proceeding in the same way, the steady state solution of x_2^{*d} (Mdm2) can be obtained as a function of x_{11}^*. The result is given by,

$$x_2^{*d}(x_{11}^*)\sim\rho\left(\frac{\epsilon}{x_{11}^*}-1\right) \tag{32}$$

where, $\rho=\frac{k_{22}}{k_{18}}$ and $\epsilon=\frac{k_{24}}{k_{22}}$ are constants. It can also be seen from the equation (32) that $x_2^{*d}\propto k_{22}$ (k_{22} is degradation rate of HDAC1). Further for positive x_2^{*d}, we have the condition $x_{11}^*<\epsilon=\frac{k_{24}}{k_{22}}$ which means that the creation rate of HDAC1 (k_{24}) should be larger than degradation rate of HDAC1 (k_{22}) provided the condition. This behaviours can be seen in Fig. 8.

Next we solve for steady state solution x_2^{*d} of $Mdm2$ as a function of x_8^* (steady state solution of p300) to study the impact of p300 on Mdm2. The result is given by,

$$x_2^{*d}(x_8^*) \sim c\left(\frac{a-x_8^*}{x_8^*-b}\right) \tag{33}$$

where, $c=\frac{k_{22}k_{18}}{k_{20}k_{22}+k_{18}}$, $ba\frac{k_{23}}{k_{18}}$ and $b=\frac{k_{23}-k_{18}k_{24}}{k_{18}+k_{20}k_{22}}$ are constants. From equation (33) for positive x_2^{*d} one can either $a\rangle x_8^*$ and $x_8^*\rangle b$ or $a\langle x_8^*$ and $x_8^*\langle b$. Moreover b to be positive the condition $k_{24}\langle\frac{k_{23}}{k_{18}}$ should be satisfied.

Now we solve steady state solution of x_1^{*d} as a function of x_8^* to understand the impact of p300 on p53. The result is given by,

$$x_1^{*d}(x_8^*) \sim s x_2^{*d}(x_8^*)\left(u+x_8^*+\frac{v}{w+x_2^{*d}(x_8^*)}\right) \tag{34}$$

where, $s=\frac{k_4k_{20}}{k_2k_3}$, $u=\frac{k_5}{k_{20}}$, $v=\frac{k_{24}}{k_{20}}$ and $w=\frac{k_{22}}{k_{18}}$ are constants. $x_2^{*d}(x_8^*)$ is given by the equation (33). The equation (34) indicates that x_1^{*d} is increased by increase in x_8^* but decrease in x_2^{*d}. Further if k_{24}, the sysnthesis rate of HDAC1 is increased then x_1^{*d} will also be increased. It can also be seen from s and (34) that $x_1^{*d}\propto\frac{1}{k_2}$ (synthesis rate of Mdm2).

The role of noise and stabilization on $p53-Mdm2$ regulation

Now we present the role of noise on $p53$ and $Mdm2$ dynamics. This is done by solving the CLE equations (16)-(29) numerically. The results for different system size parameter, V (1-50) at constant values of k_{p300} and k_{HDAC1}, are shown in Fig. 14 (a)–(f). It has been observed that for $V=1$, no oscillation in $p53$ is seen. However, as V increases the oscillation starts emerging and when $V=25$ and 50 sustained oscillations are observed with increasing $p53$ level. After $V=50$ i.e. for $V\geq 50$, the $p53$ level remains constant i.e. it exhibits sustained oscillatory behaviour. The $p53$ dynamics is noise induced stochastic process and the strength of noise decreases as V increases. The same behaviour is also seen in $Mdm2$ dynamics keeping all conditions the same (Fig. 14 (a)–(f)).

Now we present the impact of $p300$ on $p53$ and $Mdm2$ in stochastic system by simulating $p53$ and $Mdm2$ levels as a function of k_{p300} for different V (Fig. 15). The result for $V=10$ shows similar pattern as we found in the deterministic case, but the two conditions of stabilization and activation is achieved earlier with respect to k_{p300} in stochastic case than that of the deterministic case as shown in the insets of the Fig. 15. Further, as one increases V, the values k_{p300} for getting the two conditions of stabilization and activation are increased.

The dynamics of $p53$ concentration remains constant with small fluctuations around the constant values of $V(\sim 1-15)$ even though there is a small damping behavior at initial few hours. We then define T_V as the critical time below which the dynamics either shows damped or fixed point (stabilized) oscillations. The plot (T_V-V) in Fig. 16 shows the damped, stabilized and oscillatory regimes. To generate this plot we took 50 simulations for a certain fixed set of parameters and points in the curves show average values with error bars which are correct up to of the order

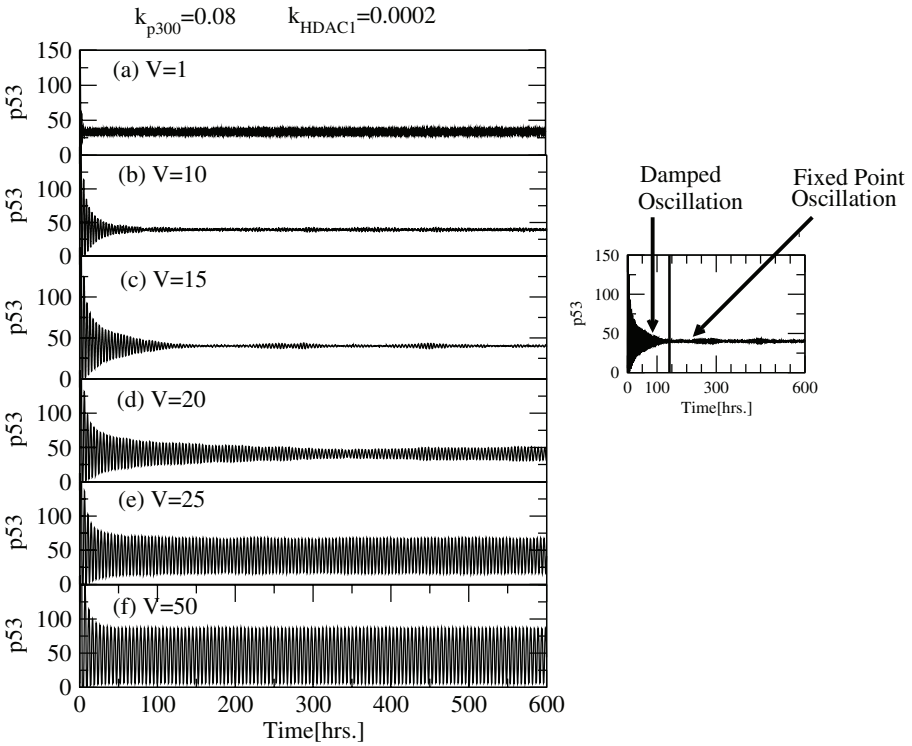

Figure 14. Noise contribution on $p53$ dynamics in stochastic system. The variation of $p53$ as a function of time in hours in stochastic system for different values of system size, $V=1$, 10, 15, 20, 25, 50 (at constant values of $k_{p300}=0.08$ and $k_{HDAC1}=0.0002$).
doi:10.1371/journal.pone.0052736.g014

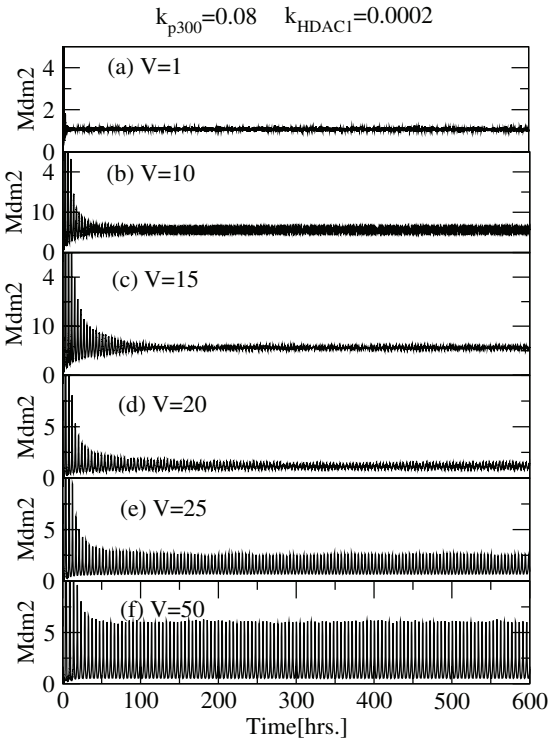

Figure 15. Noise contribution on *Mdm2* dynamics in stochastic system. The variation of *Mdm2* as a function of time in hours in stochastic system for different values of system size, $V = 1$, 10, 15, 20, 25, 50 (at constant values of $k_{p300} = 0.08$ and $k_{HDAC1} = 0.0002$).
doi:10.1371/journal.pone.0052736.g015

of 5-10 percent in our calculation as shown in Fig. 16. The plots show how system size, which can be taken as noise parameter (as V increases noise strength decreases and vice versa), drives the system at different states, namely, damped, stabilized (no oscillation) and sustain oscillation regimes.

We also study the impact of exposure time (η) on *p53* activation and stabilization for different values of V keeping the value of η constant. We can see from the two left panels with insets in Fig. 15 that as η increases the conditions of stabilization and activation are obtained faster.

The results showing the impact of *p300* on *p53* in stochastic system for different Vs and ηs are presented in Fig. 17. We also get the similar behaviour in the case as obtained in the case of *Mdm2* as shown in Fig. 18.

Stochastic steady state solutions: the noise effect

The steady state solutions of CLE can also be obtained as we did in deterministic case from the equations (17)–(30). We first impose steady state condition to the set of CLEs i.e. $dx_i/dt = 0$ and got a set of steady state equations which are very difficult to solve. However, the steady state solutions can be obtained if we neglect negligible terms which have $O(\xi^2)$ and $O(V^{-2})$ and rearrange the terms to solve the equations. Then one can easily solve simplified steady state equations. Proceeding in this way, the stochastic steady state solution of x_1^{*s} as a function of x_{11}^* is obtained and given by,

$$x_1^{*s}(x_{11}^*, V, \xi_i) \sim x_1^{*d}(x_{11}^*) + \Lambda(x_{11}^*, V)\xi_i \tag{35}$$

where, $x_1^{*d}(x_{11}^*)$ is given by equation (31) and we have taken the noise parameters $\{\xi\}$ associated with each noise term are taken to be the same as ξ_i. The noise term $\Lambda(x_{11}^*, V)$ is given by,

$$\Lambda(x_{11}^*, V) \sim \frac{A}{\sqrt{V}}\left[(q_1 - q_2\sqrt{\epsilon - x_{11}^*})\left(1 - \frac{q_3}{x_{11}^*}\right) + \sqrt{k_5\rho\left(\frac{\epsilon}{x_{11}^*} - 1\right)}\right] + \frac{A}{\sqrt{V}}\left[\sqrt{k_{18}\rho(\epsilon - x_{11}^*)} + q_4\left(1 + q_5 x_{11}^* + \frac{q_6}{x_{11}^*}\right)\right] \tag{36}$$

where, $A = \frac{k_4}{k_2 k_3}$, $q_1 = \frac{k_2 k_{20}\sqrt{k_{23}}}{k_{14} - k_{20}\rho}$, $q_2 = \frac{k_2 k_{20}\sqrt{k_{18}\rho}}{k_{14} - k_{20}\rho}$, $q_3 = \frac{k_{20}\rho\epsilon}{k_{14} - k_{20}\rho}$, $q_4 = \sqrt{k_{23} - k_{18}\rho\epsilon}\left[1 + \frac{k_{14}}{2k_{20}\rho} + \frac{k_{14}k_{18}\epsilon}{2k_{20}(k_{23} - k_{18}\rho\epsilon)}\right]$,

$$q_5 = \frac{\left(1 + \frac{k_{14}}{2k_{20}\rho}\right)\left(\frac{k_{18}\rho}{k_{23} - k_{18}\rho\epsilon}\right)}{1 + \frac{k_{14}}{2k_{20}\rho} + \frac{k_{14}k_{18}}{2k_{20}(k_{23} - k_{18}\rho\epsilon)}},$$ and

$$q_6 = \frac{k_{14}\epsilon}{2k_{20}\rho\left[1 + \frac{k_{14}}{2k_{20}\rho} + \frac{k_{14}k_{18}\epsilon}{2k_{20}(k_{23} - k_{18}\rho\epsilon)}\right]}$$ are constants. It

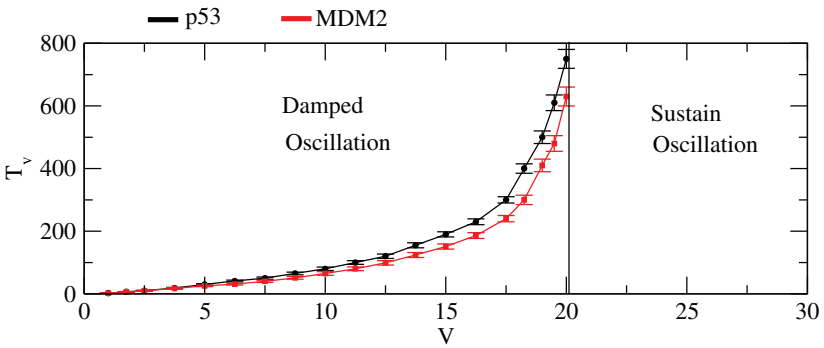

Figure 16. Phase diagram on *p53* and *Mdm2* dynamics in stochastic system. Phase diagram indicating damped and sustained oscillation regimes induced by system size, V.
doi:10.1371/journal.pone.0052736.g016

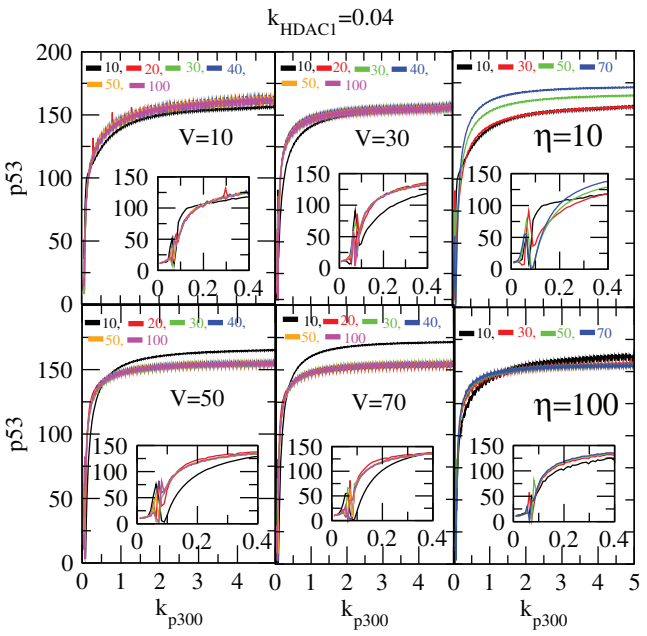

Figure 17. Stabilization of *p53* in stochastic system. (a) Plots of *p53* concentration levels as a function of *p300* for different values of system size, V = 10, 30, 50 and 70 and for different values of η = [10–100] as shown in the four left panels. The insets show the enlarged portions of the activated regimes in each case. (b) Plots of *p53* level versus k_{p300} for different V = 10, 30, 50, 70 and for two different values of η = 10 and 100 respectively as shown in two right hand panels.
doi:10.1371/journal.pone.0052736.g017

can be seen from equation (36) that the terms apart from first term and last terms in the last paranthesis will contribute to Λ only when $x_{11}^* < \epsilon$. Hence for $x_{11}^* > \epsilon$, the equation (36) will have the following expression,

$$A(x_{11}^*, V) \sim \frac{A}{\sqrt{V}}\left[e + f x_{11}^* + \frac{g}{x_{11}^*}\right] \tag{37}$$

where, $e = q_1 + q_2$, $f = q_4 q_5$ and $g = q_4 q_6 - q_1 q_3$. It can also be seen from A and equation (36)-(37)that $\Lambda \propto \frac{1}{k_2}$.

Next we calculated the steady state solution of x_2^{*d} as a function of x_{11}^*. The result can be expressed along with the deterministic result as shown in equation (32) with noise term. It is given by,

$$x_2^{*s}(x_{11}^*) \sim \frac{1}{4} x_2^{*d}(x_{11}^*) - \frac{\xi_j}{4k_{18}\sqrt{V}}\left(\sqrt{\frac{k_{22}}{x_{11}}} + \frac{\sqrt{k_{24}}}{x_{11}}\right) \tag{38}$$

where, ξ_j is the random noise parameter which we have taken same for all terms involved in the derivation. The noise contribution in this case is negative to the deterministic result which reduces steady state level of x_2^{*s} as the strength of noise increases. Further the increase in degradation and synthesis rate of HDAC1 (k_{22}) lead to increase in noise contribution which in turn decreases x_2^{*s}.

Similarly, the stochastic steady state solutions of x_1^{*s} and x_2^{*s} as a function of x_8^* along with their respective deterministic solutions given by equations (33) and (34) can also be calculated. The results are given by,

$$x_1^{*s}(x_8^*) \sim x_1^{*d}(x_8^*) + \chi(x_8^*, V)\xi_k \tag{39}$$

and

$$x_2^{*s}(x_8^*) \sim x_2^{*d}(x_8^*)\left[1 - \frac{h}{x_8^* - b}\frac{\xi_l}{\sqrt{V}}\right] \tag{40}$$

where, ξ_k and ξ_l are random noise parameters for equations (39) and (40) respectively. The function χ is given by

$$\chi(x_8^*, V) \sim \frac{1}{\sqrt{V}}\left[\frac{h x_2^{*d}}{x_8^* - b}\left(\frac{\lambda x_2^{*d}}{w + x_2^{*d}} - k_{20}x_8^* - k_5\right) + \frac{\eta}{w + x_2^{*d}}\right]$$

$$+ \frac{\phi}{\sqrt{V}}\left[\sqrt{x_2^{*d}} + \sqrt{k_{20}x_8^*} + \sqrt{\frac{k_{24}}{w + x_2^{*d}}}\right] \tag{41}$$

where, $h = \frac{k_{18}\sqrt{k_{24}}}{k_{20}k_{22} + k_{18}}$, $\lambda = k_{18}k_{24}$, $\eta = k_{24} + \sqrt{k_{24}}$ and $\phi = \frac{k_4}{k_2 k_3}$ are constants. The noise function χ is mainly contributed from first, 5th and 6th terms in equation (41) and χ is positive contributor to the deterministic part. From these main contribut-

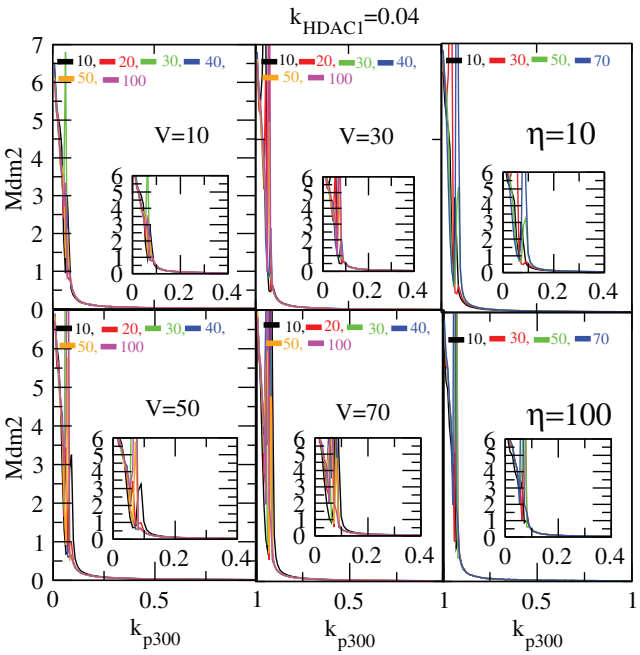

Figure 18. Stabilization of *Mdm2* in stochastic system. (a) Plots of *Mdm2* concentration levels as a function of *p300* for different values of system size, V = 10, 30, 50 and 70 and for different values of η = [10–100] as shown in the four left panels. The insets show the enlarged portions of the activated regimes in each case. (b) Plots of *Mdm2* level versus k_{p300} for different V = 10, 30, 50, 70 and for two different values of η = 10 and 100 respectively as shown in two right hand panels.
doi:10.1371/journal.pone.0052736.g018

ing terms, the synthesis rate of HDAC1, x_2^{*d} and x_8^* and their variation give significant contributions to the noise terms in equations (39) and (40). However noise contribution in equation (40) is negative contributor to the deterministic part.

Conclusion

The interaction of $p300$ with $p53$ allows $p53$ to be acetylated which prohibits it from decaying and allows it to participate in other reactions. This excess in $p300$ level eventually leads to increase in capped $p53$ whose population cannot be controlled and subjects the cell to stress condition. If the excess in $p300$ level is strong enough it may lead to cell death due to uncontrolled $p53$, similar to cancer. We observe this phenomena in our simulation results in qualitative sense via three different stages/conditions, namely, first stabilization or normal condition where impact of $p300$ is negligible, second activation of $p53$ due to significant interaction between $p300$ and $p53$, and third uncontrolled growth of capped $p53$ due to interaction with excess $p300$ leading to second stabilization level which may represent cell death condition. The same behaviour is seen in $Mdm2$ simulation results. The three conditions of stabilization and activation are obtained but the second stabilization level is obtained at lower level as compared to first stabilization level. This may be due to the fact that the increase of capped $p53$ cannot activate $Mdm2$ as is done normally, and goes to lower minimum level.

The interaction of $HDAC1$ with $p53$ will cause deacetylation of capped $p53$ which leads $p53$ to participate in other reactions and able to decay. This may help the already stressed cell to bring back to its normal condition. However excess of $HDAC1$ will cause excess deacetylation of $p53$ and will allow the cell to come back far beyond to its normal condition leading to stress. Our results supports these findings.

Noise has interesting but contrasting roles in stochastic system depending upon its strength. If its strength is strong then it has destructive impact on the signal processing in and outside the system etc. However if its strength is weak then it exhibit constructive role, for example weak signal detection, amplification and processing the signal etc. In our study, we found that if the system size is very small where the noise strength is very strong with respect to system size, the associated noise destroy the signal in the system which is in agreement with the theoretical claim. But if the system size is increased in our study where noise strength is comparatively weaker, the signal is resumed in normal with noise induced dynamics in each variable. Moreover, in stochastic system, the $p53/Mdm2$ is activated by small concentration level of $p300/HDAC1$ as compared to those in deterministic case and reach stabilization much much faster as compared to deterministic system. Further increase in system size reduces the noise fluctuation in the dynamics of each variable and when $V \to \infty$, the noise strength is negligible and the system goes to classical deterministic system.

In the present study we determine only the impact of $p300$ and $HDAC1$ on $p53-Mdm2$ regulatory network. For developing any realistic model one needs to incorporate other proteins which influence $p53$ protein simultaneously and then study the impact collectively. Our study is just one step forward towards understanding p53 regulatory network.

Acknowledgments

RKBS and Md. J. Alam gratefully acknowledge University Grants Commission (UGC) for the financial support to carry out some part of this work.

Author Contributions

Conceived and designed the experiments: RKBS SMA. Constructed the model and performed the simulation: AA SG TM DR MJA RKBS SMA. Did the analysis of the simulation: AA SG TM DR MJA RKBS SMA. Wrote the paper: AA SG TM DR MJA RKBS SMA.

References

1. Toledo F, Wahl GM (2006) Regulating the p53 pathway: in vitro hypotheses, in vivo veritas. Nat Rev Cancer 6: 909–23.
2. Lane DP (1992) p53, guardian of the genome. Nature 358: 15–16. doi:10.1038/358015a0.
3. Vousden KH (2000) p53: death star. Cell 103: 691–4.
4. Levine AJ (1997) p53, the cellular gatekeeper for growth and division. Cell 88: 323–31.
5. Bai L, Zhu W-G (2006) p53: Structure, Function and Therapeutic Applications. J. Cancer Mol. 2: 141–153.
6. Finlay CA (1993) The mdm-2 oncogene can overcome wild-type p53 suppression of transformed cell growth. Mol Cell Biol 13: 301–6.
7. Carter S, Vousden KH (2008) p53-Ubl fusions as models of ubiquitination, sumoylation and neddylation of p53. Cell Cycle 7: 2519–2528.
8. Lambert PF, Kashanchi F, Radonovich MF, Shiekhattar R, Brady JN (1998) Phosphorylation of p53 serine 15 increases interaction with CBP. J Biol Chem. 273: 33048–53.
9. Grossman SR, Perez M, Kung AL, Joseph M, Mansur C, et al. (1998) p300/MDM2 complexes participate in MDM2-mediated p53 degradation. Mol Cell. 2: 405–415.
10. Zeng X, Chen L, Jost CA, Maya R, Keller D, et al. (1999) MDM2 suppresses p73 function without promoting p73 degradation. Mol Cell Biol.19: 3257–66.
11. Meek DW, Anderson CW (2009) Posttranslational Modification of p53: Cooperative Integrators of Function. Cold Spring Harb. Perspect. Biol. 00: a000950.
12. Leslie PH (1958) A Stochastic Model for Studying the Properties of Certain Biological Systems by Numerical Methods. Biometrika 45: 16–31.
13. Gillespie DT (1977) Exact stochastic simulation of coupled chemical reactions. J. Phy. Chem. 31: 2340–2361.
14. Mc Quarrie DA (1967) Stochastic approach to chemical kinetics. J. Appl. Probab. 4: 413.
15. Anishchenko VS, Neiman AB, Moss F, Schimansky-Geier L (1999) Stochastic resonance: noise-enhanced order. Physcs-Uspekhi 42: 7–36.
16. Hanggi P (2002) Stochastic resonance in biology how noise can enhance detection of weak signals and help improve biological information processing. ChemPhysChem 3: 285–290.
17. Blake WJ, Kaern M, Cantor CR, Collins JJ (2003) Noise in eukaryotic gene expression. Nature 422: 633637.
18. Becskei A, Seraphin B, Serrano L (2001) Positive feedback in eukaryotic gene networks: cell differentiation by graded to binary response conversion. EMBO J 20: 25282535.
19. Weinberger LS, Burnett JC, Toettcher JE, Arkin AP, Schaffer DV (2005) Stochastic gene expression in a lentiviral positive-feedback loop: HIV-1 Tat fluctuations drive phenotypic diversity. Cell 122: 169182.
20. Kussell E, Leibler S (2005) Phenotypic diversity, population growth, and information in fluctuating environments. Science 309: 20752078.
21. Kubbutat MHG, Jones SN, Vousden KH (1997) Regulation of p53 stability by Mdm2. Natute 387: 299.
22. Proctor CJ, Gray DA (2008) Explaining oscillations and variability in the p53-Mdm2 system. BMC Systems Biol. 2:75. doi:10.1186/1752-0509-2-75.
23. Rodriguez MS, Desterro JMP, Lain S, Lane DP, Hay RT (2000) Multiple C-Terminal Lysine Residues Target p53 for Ubiquitin-Proteasome-Mediated Degradation. Mol. Cell Biol. 20: 8458.
24. Grossman SR, Deato ME, Brignone C, Chan HM, Kung AL, et al. (2003) Polyubiquitination of p53 by p300. Science 300: 342–344.
25. Wagner J, Ma L, Rice JJ, Hu W, Levine AJ, et al. (2005) p53-Mdm2 loop controlled by a balance of its feedback strength and effective dampening using ATM and delayed feedback. IEE Proc-Syst. Biol. 152: 109.
26. Dumaz N, Meek DW (1999) Serine 15 phosphorylation stimulates p53 transactivation but does not directly influence interaction with HDM2. EMBO J. 18: 7002.
27. Gu W, Roeder RG (1997) Activation of p53 Sequence-Specific DNA Binding by Acetylation of the p53 C-Terminal Domain. Cell 90: 595–606.
28. Kobet E, Zeng X, Zhu Y, Keller D, Lu H (2000) MDM2 inhibits p300-mediated p53 acetylation and activation by forming a ternary complex with the two proteins. Proc. Nat. Acad. Sc. 97: 1254712552.
29. Ito A, Lai CH, Zhao X, Saito S, Hamilton MH, et al. (2001) p300/CBP-mediated p53 acetylation is commonly induced by p53-activating agents and inhibited by MDM2: EMBO J. 20: 1331–40 (2001).

30. Knights CD, Catania J, Di Giovanni S, Muratoglu S, Perez R (2006) Distinct p53 acetylation cassettes differentially influence gene-expression patterns and cell fate: J Cell Biol. 173: 533–44.
31. Luo J, Li M, Tang Y, Laszkowska M, Roeder RG, et al. (2004) Acetylation of p53 augments its site-specific DNA binding both in vitro and in vivo: Proc. Natl. Acad. Sc. 101: 2259–2264.
32. Li, Luo J, Brooks CL, Gu W (2002) Acetylation of p53 Inhibits Its Ubiquitination by Mdm2. J Biol Chem. 277: 50607–50611.
33. Ito A, Kawaguchi Y, Lai CH, Kovacs JJ, Higashimoto Y, et al. (2002) MDM2HDAC1-mediated deacetylation of p53 is required for its degradation. The EMBO J. 21: 6236–6245.
34. Pavithra L, Mukherjee S, Sreenath K, Kar S, Sakaguchi K, et al. (2009) SMAR1 Forms a Ternary Complex with p53-MDM2 and Negatively Regulates p53-mediated Transcription. J. Mol. Biol. 388: 691.
35. Gillespie DT (2007) Stochastic simulation of chemical kinetics. Annu. Rev. Phys. Chem., 58: 35.
36. van-Kampen NG (2007) Stochastic processes in Physics and Chemistry. Elsevier, New York.
37. Bratsun D, Volfson D, Tsimring LS, Hasty J (2005) Delay-induced stochastic oscillations in gene regulation. Proc. Nat. Acad. Sc. 102:14593–14598.
38. Cai X (2007) Exact stochastic simulation of coupled chemical reactions with delays. J. Chem. Phys. 126:124108.
39. Gillespie DT (2001) Approximate accelerated stochastic simulation of chemically reacting systems. J. Chem. Phys. 115: 1716.
40. Salis H, Kaznessis Y (2000) Accurate hybrid stochastic simulation of a system of coupled chemical or biochemical reactions. J. Chem. Phys. 122: 054103.
41. Gillespie DT (2000) The chemical Langevin equation. J. Chem. Phys. 113: 297.
42. Press WH, Teukolsky SA, Vetterling WT, Flannery BP (1992) Numerical Recipe in Fortran. Cambridge University Press.
43. Ciliberto A, Novak B, Tyson JJ (2005) Steady states and oscillations in the p53/Mdm2 network. Cell Cycle. 4: 488–493.
44. Lev Bar-Or R, Maya R, Segel LA, Alon U, Levine AJ, et al. (2000) Generation of oscillations by the p53-Mdm2 feedback loop: a theoretical and experimental study. Proc Natl Acad Sci 97: 11250–11255.
45. Zhang T, Brazhnik P, Tyson JJ (2007) Exploring mechanisms of the DNA-damage response: p53 pulses and their possible relevance to apoptosis. Cell Cycle. 6: 85–94.
46. Lahav G, Rosenfeld N, Sigal A, Geva-Zatorsky N, Levine AJ, et al. (2004) Dynamics of the p53-Mdm2 feedback loop in individual cells. Nat Genet. 36: 147–150.
47. Juan LJ, Shia WJ, Chen MH, Yang WM, Seto E, et al. (2000) Histone deacetylases specifically down-regulate p53-dependent gene activation. J Biol Chem. 275: 20436–20443.
48. Luo J, Su F, Chen D, Shiloh A, Gu W, et al. (2000) Deacetylation of p53 modulates its effect on cell growth and apoptosis. Nature 408: 377–381.